Asian Journal of Chemistry; Vol. 38, No. 5 (2026), 1324-1332

ASIAN JOURNAL OF CHEMISTRY

https://doi.org/10.14233/ajchem.2026.35287

Design and Synthesis of Novel Hydrazone-Linked 1,2,3-Triazole-Pyrazole Derivatives: *In vitro* Cytotoxicity, Antimicrobial and Molecular Docking Studies

POTHARAJU SUNIL KUMAR, RAMBABU BHUKYA, CHANDULAL BHUKYA, NAMPALLY RAJITHA, GOLI J. RUPASREE, NALAPARAJU NAGARAJU and RAMCHANDER JADHAV*

Department of Chemistry, University College of Science, Osmania University, Hyderabad-500007, India

*Corresponding author: E-mail: ramorgchemou@gmail.com

Received: 15 November 2025 *Accepted*: 10 April 2026 *Published online*: 4 May 2026 AJC-22358

A series of novel hydrazone-linked 1,2,3-triazole-pyrazole derivatives (**7a-l**) were rationally designed and synthesised through an efficient multistep synthetic strategy. The key intermediates were constructed *via* diazotisation–azidation followed by cycloaddition to generate the 1,2,3-triazole core, which was further functionalised to afford the target hydrazone derivatives. Final compounds were evaluated for their *in vitro* anticancer and antimicrobial activities. Antiproliferative screening against selected human cancer cell lines revealed that compounds bearing electron-withdrawing substituents exhibited superior cytotoxicity compared to electron-donating analogues. Among the synthesised derivatives, **7d** (*p*-Cl) and **7c** (*p*-NO_2) exhibited the lowest IC_{50} values against the MCF-7 cell line (0.10 and 0.55 μM, respectively), comparable to doxorubicin (0.92 μM) under the same conditions. In antibacterial assays, halogen and fluoro-substituted derivatives demonstrated comparatively improved activity, with compounds **7b**, **7d**, **7i** and **7k** showing notable potency. Antifungal evaluation revealed that nitro-, fluoro- and methoxy-substituted analogues, particularly **7c**, **7e** and **7f**, displayed enhanced activity against the tested strains. Molecular docking studies suggested favourable binding interactions with selected biological targets. Based on the obtained results, it is concluded that hydrazone-linked 1,2,3-triazole-pyrazole hybrids act as promising scaffolds for further optimisation toward anticancer and antimicrobial applications.

Keywords: Hydrazone derivatives, 1,2,3-Triazole-pyrazole hybrids, Cytotoxicity activity, Antimicrobial activity, Molecular docking.

INTRODUCTION

Among privileged heterocycles, 1,2,3-triazoles occupy a central position due to their metabolic stability, strong dipole character and capacity to participate in hydrogen-bonding and π-interactions with biological macromolecules [1-3]. Extensive studies have demonstrated that 1,2,3-triazole-containing hybrids can display diverse pharmacological profiles including antiproliferative and antimicrobial effects and they are frequently explored alongside *in silico* techniques such as molecular docking to rationalize structure-activity relationships (SAR) [4-7].

Likewise, the pyrazole nucleus is a well-established bioactive scaffold found in numerous lead structures and drug like candidates, with reported antibacterial, antifungal and anticancer potential [8-10]. Recent literature highlights that the strategic substitution and hybrid formation, particularly coupling pyrazole with other heterocyclic systems, can significantly modulate biological profiles and target affinity [11-13]. In this context, triazole-pyrazole hybrids have attracted sustained attention, with several reports describing compounds exhibiting potent antimicrobial activity and/or cytotoxicity against various cancer cell lines [14-16].

In parallel, hydrazones are also recognised as versatile pharmacophores and valuable synthetic intermediates, offering conformational flexibility and multiple hydrogen bond donor/acceptor sites that facilitate the interaction with enzymes and receptors [17,18]. Hydrazone-containing compounds have been widely investigated for their antimicrobial and antiproliferative activities and recent reviews continue to underscore their importance as promising scaffolds in drug discovery [19-21]. Notably, triazole-linked hydrazones and related hybrid systems have demonstrated significant biological potential, with molecular docking studies frequently employed to support mechanistic insights and guide the structural optimisation [22,23].

Hydrazones, 1,2,3-triazoles and pyrazoles represent privileged pharmacophores in medicinal chemistry, as evidenced by their presence in numerous clinically approved drugs across diverse therapeutic areas. Hydrazone- and hydrazide-based motifs are integral to several important drugs including isoniazid and hydralazine for tuberculosis and hypertension, respectively, as well as anticancer agents such as procarbazine and dacarbazine, highlighting their relevance in both antimicrobial and antiproliferative therapy [24-27]. Similarly, the triazole scaffold has achieved remarkable success in drug discovery owing to its metabolic stability and favourable binding characteristics, with triazole-containing drugs such as fluconazole, itraconazole, voriconazole and posaconazole being widely used as frontline antifungal agents, while other triazole-based drugs like ribavirin, ticagrelor, alprazolam and triazolam demonstrate antiviral, antiplatelet and central nervous system activities [28-32]. In parallel, the pyrazole nucleus is a well-established structural motif in several marketed drugs, particularly in anti-inflammatory and anticancer therapy. Notable examples include celecoxib and phenylbutazone as anti-inflammatory agents and kinase inhibitors such as crizotinib, ruxolitinib, pazopanib and tofacitinib, which are widely used in cancer and immunological disorders [33-38]. The broad spectrum of biological activities associated with these scaffolds underscores their excellent drug-likeness and validates ongoing efforts to develop hybrid molecules that integrate hydrazone, triazole and pyrazole pharmacophores within a single molecular framework to achieve enhanced antiproliferative and antimicrobial efficacy [39-41].

Based on these considerations, the present work focuses on the design, synthesis and characterisation of hydrazone-linked 1,2,3-triazole-pyrazole derivatives, followed by evaluation of their *in vitro* antiproliferative and antimicrobial activities, along with molecular docking studies to elucidate plausible binding modes and key ligand–target interactions, thereby supporting SAR-driven lead identification and further optimisation.

EXPERIMENTAL

All the synthetic reagents, catalysts and solvents were obtained from reputable chemical suppliers such as Merck, Sigma-Aldrich, TCI, Spectrochem and Avra Chemicals. These chemicals were used directly without any additional purification. The progress of the reactions was monitored by thin-layer chromatography (TLC) on Merck silica gel 60 F_{254} plates. Melting points of the final compounds were determined using a Stuart SMP3 apparatus and the values are uncorrected. Purification of the crude mixtures was carried out through recrystallisation and by column chromatography using ethyl acetate and *n*-hexane in a 10:90 ratio as the eluent system. The composition and functional groups of the synthesised compounds were confirmed by infrared spectroscopy using a Shimadzu FTIR 8400 S instrument with KBr pellets. ^{1}H and ^{13}C NMR spectra were recorded on a Bruker 400 MHz spectrometer operating at 400 MHz and 100 MHz, respectively, with $CDCl_3$ and DMSO-d_6 as solvents and TMS as the internal reference. Mass spectral data were obtained using a Shimadzu GC-MS QP 1000 system.

Synthesis: The synthesis of novel hydrazone-linked 1,2,3-triazole-pyrazole derivatives (**7a-l**) was accomplished through a multistep protocol involving diazotisation, cycloaddition and condensation reactions. Initially, aromatic anilines (**1a-l**) were converted into the corresponding aryl azides (**2a-l**), which were subsequently subjected to a base-catalysed reaction with a 1,3-dicarbonyl compound (2,4-diketone) to furnish the desired 1,2,3-triazole derivatives. The corresponding carbaldehyde (**5a-l**) were then obtained *via* a two-step synthetic sequence. In first step, hydrazone derivatives (**4a-l**) were prepared by the condensation of the appropriate ketones (**3a-l**) with phenylhydrazine in absolute ethanol, using a catalytic amount of glacial acetic acid. The reaction mixture was stirred at room temperature for 2-3 h and the progress of the reaction was monitored by TLC. Upon completion, hydrazones were isolated by standard work-up procedures. In the subsequent step, the synthesised hydrazones (**4a-l**) were subjected to formylation using the Vilsmeier–Haack reagent, generated *in situ* from DMF and $POCl_3$, to afford the corresponding carbaldehyde (**5a-l**) in good yields. Finally, the carbaldehyde derivatives (**5a-l**) were condensed with benzenesulfonyl hydrazide in absolute ethanol in the presence of a catalytic amount of glacial acetic acid (**Scheme-I**). The reaction mixture was stirred at room temperature for 4 h and the progress of the reaction was monitored by TLC. Upon completion, the products were isolated to afford the corresponding hydrazone derivatives (**7a-l**) in good yields.

(*Z*)-4-Methyl-*N′*-((3-(5-methyl-1-(*p*-tolyl)-1*H*-1,2,3-triazol-4-yl)-1-phenyl-1*H*-pyrazol-4-yl)methylene)benzenesulfonohydrazide (7a): White solid; yield: 75%, m.p.: 188-190 ºC; IR (KBr, ν_{max}, cm^{-1}): 3169 (N-H), 3090 (=C-H), 1715 (C=N imine), 1554 (C=C), 1264 (N=N), 1204 (S=O); ^{1}H NMR (500 MHz, $CDCl_3$, δ ppm): 8.72 (s, 1H), 8.48 (s, 1H), 7.86 (d, *J* = 8.3 Hz, 2H), 7.76 (d, *J* = 9.4 Hz, 2H), 7.50 (t, *J* = 8.0 Hz, 2H), 7.38-7.33 (m, 6H), 7.30 (d, *J* = 8.1 Hz, 2H), 2.64 (s, 3H), 2.47 (s, 3H), 2.39 (s, 3H); ^{13}C NMR (500 MHz, $CDCl_3$, δ ppm): 144.34, 143.97, 142.31, 139.95, 139.43, 138.58, 135.64, 133.58, 132.48, 130.17, 129.67, 129.58, 127.92, 127.16, 125. ESI-MS: *m/z* 512 [M+H]$^+$; Elemental analysis: calcd. (found) %: C, 63.39 (63.34); H, 4.93 (4.87); N, 19.17 (19.11).

(*Z*)-*N′*-((3-(1-(4-Bromophenyl)-5-methyl-1*H*-1,2,3-triazol-4-yl)-1-phenyl-1*H*-pyrazol-4-yl)methylene)-4-methylbenzenesulfonohydrazide (7b): White solid; yield: 64%, m.p.: 186-188 ºC; IR (KBr, ν_{max}, cm^{-1}): 3154 (N-H), 3086=C-H), 1685 (C=N), 1545 (C=C), 1252 (N=N), 1165 (S=O); ^{1}H NMR (500 MHz, $CDCl_3$, δ ppm): 8.68 (s, 1H), 8.47 (s, 1H), 7.86 (d, *J* = 8.3 Hz, 2H), 7.76 (d, *J* = 7.8 Hz, 2H), 7.72 (d, *J* = 8.6 Hz, 2H), 7.50 (t, *J* = 7.9 Hz, 2H), 7.40 (d, *J* = 8.6 Hz, 2H), 7.35 (t, *J* = 7.4 Hz, 1H), 7.30 (d, *J* = 8.2 Hz, 2H), 2.66 (s, 3H), 2.39 (s, 3H); ^{13}C NMR (101 MHz, $CDCl_3$, δ ppm): 144.07, 142.06, 139.38, 138.99, 135.58, 135.05, 132.91, 132.36, 129.70, 129.61, 127.92, 127.28, 126.67, 125.86, 123.85, 119.06, 117.49, 21.61, 10.37. ESI-MS: *m/z* 576.2 [M+H]$^+$, Elemental analysis: calcd. (found) %: C, 54.17 (54.11); H, 3.85 (3.79); N, 17.01 (16.95).

(*Z*)-4-Methyl-*N′*-((3-(5-methyl-1-(4-nitrophenyl)-1*H*-1,2,3-triazol-4-yl)-1-phenyl-1*H*-pyrazol-4-yl)methylene)benzenesulfonohydrazide (7c): Light yellow solid, yield:

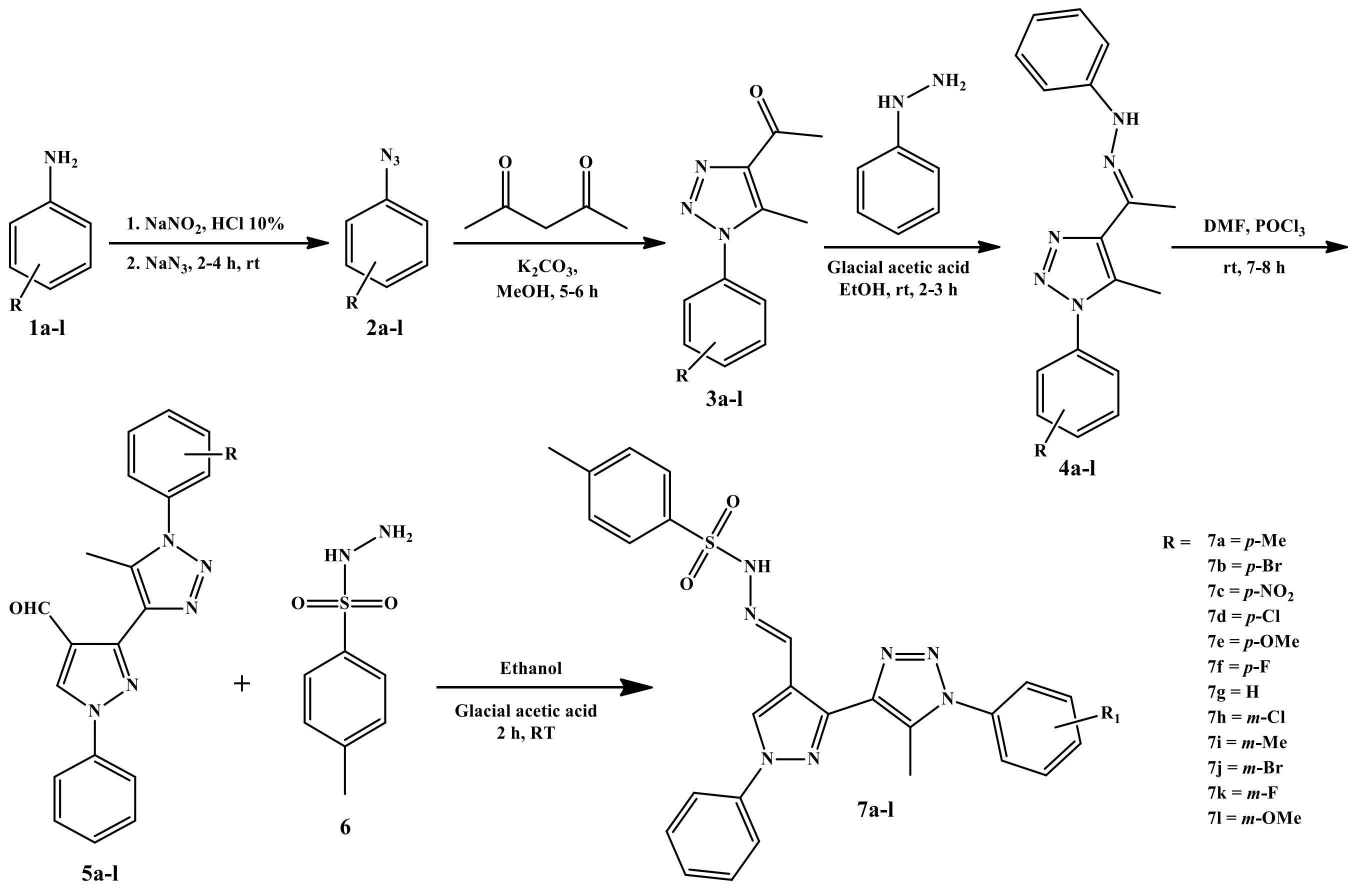

Scheme-I: Synthesis of hydrazone-linked 1,2,3-triazole–pyrazole derivatives

66%, m.p.: 194-196 ºC; IR (KBr, ν_{max}, cm^{-1}): 3162 (N-H), 3074 (=C-H), 1694 (C=N), 1552 (C=C), 1262 (N=N), 1178 (S=O); ^{1}H NMR (500 MHz, $CDCl_3$, δ ppm): 8.66 (s, 1H), 8.48 (dd, *J* = 12.1, 6.6 Hz, 2H), 7.85 (d, *J* = 8.2 Hz, 2H), 7.78 (dd, *J* = 17.1, 8.1 Hz, 5H), 7.51 (t, *J* = 7.9 Hz, 2H), 7.40-7.35 (m, 1H), 7.31 (d, *J* = 8.1 Hz, 2H), 2.75 (s, 3H), 2.40 (s, 3H); ^{13}C NMR (101 MHz, $CDCl_3$, δ ppm): 144.34, 144.09, 142.30, 139.47, 138.79, 136.14, 135.64, 132.47, 129.74, 129.69, 129.64, 127.97, 127.25, 125.84, 125.30, 119.10, 117.50, 21.66, 10.41; ESI-MS: *m/z* 543 $[M+H]^+$; Elemental analysis: calcd. (found) %: C, 57.56 (57.50); H, 4.09 (4.03); N, 20.65 (20.59).

(*Z*)-*N′*-((3-(1-(4-Chlorophenyl)-5-methyl-1*H*-1,2,3-triazol-4-yl)-1-phenyl-1*H*-pyrazol-4-yl)methylene)-4-methylbenzenesulfonohydrazide (7d): White solid, yield: 74%, m.p.: 192-194 ºC; IR (KBr, ν_{max}, cm^{-1}): 3202 (N-H), 3021 (=C-H), 1682 (C=N), 1576 (C=C), 1264 (N=N), 1187 (S=O); ^{1}H NMR (500 MHz, $CDCl_3$, δ ppm): 8.69 (s, 1H), 8.47 (s, 1H), 7.86 (d, *J* = 8.3 Hz, 2H), 7.76 (d, *J* = 7.7 Hz, 2H), 7.56 (d, *J* = 8.7 Hz, 2H), 7.52-7.45 (m, 5H), 7.35 (t, *J* = 7.4 Hz, 1H), 7.30 (d, *J* = 8.2 Hz, 2H), 2.65 (s, 3H), 2.39 (s, 3H). ^{13}C NMR (126 MHz, $CDCl_3$, δ ppm): 143.88, 142.04, 139.30, 138.84, 135.71, 135.59, 134.48, 132.42, 129.80, 129.58, 129.51, 127.84, 127.14, 126.39, 125.77, 118.97, 117.53, 21.52, 10.26; ESI-MS: *m/z* 532 $[M+H]^+$; Elemental analysis: calcd. (found) %: C, 58.70 (58.64); H, 4.17 (4.11); N, 18.43 (18.37).

(*Z*)-*N′*-((3-(1-(4-Methoxyphenyl)-5-methyl-1*H*-1,2,3-triazol-4-yl)-1-phenyl-1*H*-pyrazol-4-yl)methylene)-4-methylbenzenesulfonohydrazide (7e): White solid, yield: 79%, m.p.: 195-197 ºC, IR (KBr, ν_{max}, cm^{-1}): 3184 (N-H), 3045 (=C-H), 1687 (C=N), 1577 (C=C), 1274 (N=N), 1179 (S=O), ^{1}H NMR (500 MHz, $CDCl_3$, δ ppm): 8.71 (s, 1H), 8.47 (s, 1H), 7.86 (d, *J* = 7.8 Hz, 2H), 7.76 (d, *J* = 7.7 Hz, 2H), 7.49 (t, *J* = 7.3 Hz, 2H), 7.40 (d, *J* = 8.3 Hz, 2H), 7.35 (d, *J* = 7.2 Hz, 1H), 7.29 (d, *J* = 7.7 Hz, 3H), 7.06 (d, *J* = 8.4 Hz, 2H), 3.89 (s, 3H), 2.61 (s, 3H), 2.38 (s, 3H); ^{13}C NMR (126 MHz, $CDCl_3$, δ ppm): 160.41, 144.30, 143.91, 142.25, 139.37, 138.41, 135.58, 132.57, 129.61, 129.51, 128.88, 127.86, 127.09, 126.60, 125.70, 118.97, 117.40, 114.67, 55.62, 21.54, 10.18; ESI-MS: *m/z* 528 $[M+H]^+$; Elemental analysis: calcd. (found) %: C, 61.47 (61.41); H, 4.78 (4.72); N, 18.58 (18.52).

(*Z*)-*N′*-((3-(1-(4-Fluorophenyl)-5-methyl-1*H*-1,2,3-triazol-4-yl)-1-phenyl-1*H*-pyrazol-4-yl)methylene)-4-methylbenzenesulfonohydrazide: (7f); White solid, yield: 72%, m.p.: 184-186 ºC; IR (KBr, ν_{max}, cm^{-1}): 3178 (N-H), 3065 (=C-H), 1681 (C=N), 1565 (C=C), 1225 (N=N), 1121 (S=O); ^{1}H NMR (500 MHz, $CDCl_3$, δ ppm): 8.69 (s, 1H), 8.48 (s, 1H), 7.88-7.80 (m, 2H), 7.76 (d, *J* = 7.7 Hz, 2H), 7.53-7.47 (m, 5H), 7.35 (s, 1H), 7.31 (d, *J* = 7.2 Hz, 2H), 2.64 (s, 3H), 2.40 (s, 3H); ^{13}C NMR (126 MHz, $CDCl_3$, δ ppm): 143.77, 141.94, 139.20, 138.74, 135.60, 135.49, 134.37, 132.32, 129.70, 129.48, 129.41, 127.74, 127.04, 126.29, 125.67, 118.87, 117.43, 21.42, 10.15; ESI-MS: *m/z* 516 $[M+H]^+$; Elemental analysis: calcd. (found) %: C, 60.57 (60.51); H, 4.30 (4.24); N, 19.02 (18.96).

(*Z*)-4-Methyl-*N*′-((3-(5-methyl-1-phenyl-1*H*-1,2,3-triazol-4-yl)-1-phenyl-1*H*-pyrazol-4-yl)methylene)benzenesulfonohydrazide (7g): White solid, yield: 75% m.p.: 190-192 ºC; IR (KBr, ν_{max}, cm^{-1}): 3193 (N-H), 3047 (=C-H), 1678 (C=N), 1554 (C=C), 1232 (N=N), 1165 (S=O); ^{1}H NMR (500 MHz, $CDCl_3$, δ ppm): 8.72 (s, 1H), 8.48 (s, 1H), 7.87 (d, *J* = 8.3 Hz, 2H), 7.77 (d, *J* = 7.7 Hz, 2H), 7.58 (t, *J* = 5.1 Hz, 3H), 7.50 (dd, *J* = 11.4, 4.6 Hz, 4H), 7.35 (s, 1H), 7.30 (d, *J* = 8.1 Hz, 2H), 2.66 (s, 3H), 2.39 (s, 3H); ^{13}C NMR (101 MHz, $CDCl_3$, δ ppm): 144.29, 144.04, 142.25, 139.43, 138.70, 136.10, 135.59, 132.43, 129.69, 129.64, 129.60, 127.93, 127.21, 125.79, 125.25, 119.05, 117.45, 21.61, 10.37; ESI-MS: *m/z* 498 [M+H]$^+$; Elemental analysis: calcd. (found) %: C, 62.76 (62.71); H, 4.66 (4.61); N, 19.71 (19.65).

(*Z*)-*N*′-((3-(1-(3-Chlorophenyl)-5-methyl-1*H*-1,2,3-triazol-4-yl)-1-phenyl-1*H*-pyrazol-4-yl)methylene)-4-methylbenzenesulfonohydrazide (7h): White solid, yield: 71%; m.p.: 184-186 ºC, IR (KBr, ν_{max}, cm^{-1}): 3191 (N-H), 3056 (=C-H), 1665 (C=N), 1526 (C=C), 1263 (N=N), 1145 (S=O); ^{1}H NMR (500 MHz, $CDCl_3$, δ ppm): 8.69 (s, 1H), 8.48 (s, 1H), 7.88-7.83 (m, 2H), 7.76 (d, *J* = 7.8 Hz, 2H), 7.56-7.49 (m, 5H), 7.43-7.41 (m, 1H), 7.36 (t, *J* = 7.4 Hz, 1H), 7.31 (d, *J* = 8.2 Hz, 2H), 2.68 (s, 3H), 2.40 (s, 3H); ^{13}C NMR (101 MHz, $CDCl_3$, δ ppm): 144.08, 142.11, 139.43, 139.04, 135.63, 132.96, 132.41, 129.75, 129.67, 127.97, 127.33, 126.73, 125.91, 123.91, 119.12, 117.54, 21.67, 10.42. ESI-MS: *m/z* 532 [M+H]$^+$; Elemental analysis: calcd. (found) %: C, 58.70 (58.64); H, 4.17 (4.11); N, 18.43 (18.37).

(*Z*)-4-Methyl-*N*′-((3-(5-methyl-1-(*m*-tolyl)-1*H*-1,2,3-triazol-4-yl)-1-phenyl-1*H*-pyrazol-4-yl)methylene)benzenesulfonohydrazide (7i): White solid, yield: 78%, m.p.: 194-196 ºC; IR (KBr, ν_{max}, cm^{-1}): 3188 (N-H), 3087 (=C-H), 1698 (C=N), 1565 (C=C), 1274 (N=N), 1169 (S=O); ^{1}H NMR (500 MHz, $CDCl_3$, δ ppm): 8.69 (s, 1H), 8.45 (s, 1H), 7.84 (d, *J* = 8.3 Hz, 2H), 7.74 (d, *J* = 8.7 Hz, 2H), 7.47 (t, *J* = 8.0 Hz, 2H), 7.36-7.30 (m, 5H), 7.27 (d, *J* = 8.1 Hz, 2H), 2.61 (s, 3H), 2.44 (s, 3H), 2.37 (s, 3H); ^{13}C NMR (126 MHz, $CDCl_3$, δ ppm): 144.41, 144.04, 142.38, 140.02, 139.50, 138.65, 135.70, 133.65, 132.55, 130.24, 129.74, 129.65, 127.99, 127.23, 125.83, 125.14, 119.10, 117.54, 21.68, 21.37, 10.38; ESI-MS: *m/z* 512 [M+H]$^+$; Elemental analysis: calcd. (found) %: C, 63.33 (63.27); H, 4.87 (4.81); N, 19.11 (19.05).

(*Z*)-*N*′-((3-(1-(3-Bromophenyl)-5-methyl-1*H*-1,2,3-triazol-4-yl)-1-phenyl-1*H*-pyrazol-4-yl)methylene)-4-methylbenzenesulfonohydrazide (7j): White solid, yield: 75%, m.p.: 193-195 ºC, IR (KBr, ν_{max}, cm^{-1}): 3179 (N-H), 3065 (=C-H), 1641 (C=N), 1562 (C=C), 1245 (N=N), 1161 (S=O); ^{1}H NMR (500 MHz, $CDCl_3$, δ ppm): 8.60 (s, 1H), 8.38 (s, 1H), 7.77 (d, *J* = 8.3 Hz, 2H), 7.67 (d, *J* = 7.7 Hz, 2H), 7.47 (d, *J* = 8.7 Hz, 2H), 7.42 (d, *J* = 7.6 Hz, 1H), 7.38 (t, *J* = 5.5 Hz, 3H), 7.26 (t, *J* = 7.4 Hz, 1H), 7.21 (d, *J* = 8.2 Hz, 2H), 2.56 (s, 3H), 2.30 (s, 3H); ^{13}C NMR (101 MHz, $CDCl_3$, δ ppm): 143.87, 141.86, 139.18, 138.79, 135.38, 134.85, 132.71, 132.16, 129.50, 129.41, 127.72, 127.08, 126.47, 125.66, 123.65, 118.86, 117.29, 21.41, 10.17; ESI-MS: *m/z* 576 [M+H]$^+$; Elemental analysis: calcd. (found) %: C, 54.17 (54.11); H, 3.85 (3.79); N, 17.01 (16.95).

(*Z*)-*N*′-((3-(1-(3-Fluorophenyl)-5-methyl-1*H*-1,2,3-triazol-4-yl)-1-phenyl-1*H*-pyrazol-4-yl)methylene)-4-methylbenzenesulfonohydrazide (7k): White solid, yield: 69%, m.p.: 196-198 ºC; IR (KBr, ν_{max}, cm^{-1}): 3186 (N-H), 3087 (=C-H), 1647 (C=N), 1562 (C=C), 1232 (N=N), 1112 (S=O); ^{1}H NMR (500 MHz, $CDCl_3$, δ ppm): 8.71 (s, 1H), 8.50 (s, 1H), 7.89 (d, *J* = 8.3 Hz, 2H), 7.86 (s, 1H), 7.79 (d, *J* = 7.8 Hz, 2H), 7.56 (dd, *J* = 10.9, 4.4 Hz, 4H), 7.52 (d, *J* = 8.2 Hz, 2H), 7.46-7.43 (m, 1H), 7.38 (t, *J* = 7.4 Hz, 1H), 7.33 (d, *J* = 8.2 Hz, 2H), 2.70 (s, 3H), 2.42 (s, 3H); ^{13}C NMR (126 MHz, $CDCl_3$, δ ppm): 144.54, 144.18, 142.52, 140.16, 139.64, 138.79, 135.84, 133.79, 132.69, 130.37, 129.88, 129.79, 128.13, 127.37, 125.97, 125.28, 119.24, 117.68, 21.51, 10.52; ESI-MS: *m/z* 516 [M+H]$^+$; Elemental analysis: calcd. (found) %: C, 60.57 (60.51); H, 4.30 (4.24); N, 19.02 (18.97).

(*Z*)-*N*′-((3-(1-(3-Methoxyphenyl)-5-methyl-1*H*-1,2,3-triazol-4-yl)-1-phenyl-1*H*-pyrazol-4-yl)methylene)-4-methylbenzenesulfonohydrazide (7l): White solid, yield: 76%, m.p.: 191-193 ºC; IR (KBr, ν_{max}, cm^{-1}): 3195 (N-H), 3082 (=C-H), 1664 (C=N), 1587 (C=C), 1246 (N=N), 1165 (S=O); ^{1}H NMR (500 MHz, $CDCl_3$, δ ppm): 8.76 (s, 1H), 8.52 (s, 1H), 7.91 (d, *J* = 7.8 Hz, 2H), 7.81 (d, *J* = 7.7 Hz, 2H), 7.54 (t, *J* = 7.3 Hz, 2H), 7.45 (d, *J* = 8.3 Hz, 2H), 7.41-7.38 (m, 1H), 7.35 (s, 2H), 7.11 (d, *J* = 8.4 Hz, 2H), 3.94 (s, 3H), 2.66 (s, 3H), 2.44 (s, 3H); ^{13}C NMR (126 MHz, $CDCl_3$, δ ppm): 160.55, 144.44, 144.05, 142.39, 139.51, 138.55, 135.72, 132.71, 129.75, 129.65, 129.02, 128.00, 127.23, 126.74, 125.84, 119.11, 117.54, 114.81, 55.76, 21.68, 10.32; ESI-MS: *m/z* 528 [M+H]$^+$; Elemental analysis: calcd. (found) %: C, 61.47 (61.41); H, 4.78 (4.72); N, 18.58 (18.52).

Cytotoxicity: The synthesised compounds **7a-l** were evaluated for their *in vitro* anticancer activity using the MTT assay, a well-established colorimetric method for assessing cell viability based on mitochondrial metabolic activity. The assay was performed against the human breast cancer cell line (MCF-7) to assess anticancer potential and the mouse fibroblast cell line (NIH/3T3) was used as a representative normal cell line to evaluate cytotoxic selectivity. The compounds were tested at a range of micromolar concentrations (12, 25, 50, 100, 200 and 400 μM) to generate dose–response curves, from which IC_{50} values were calculated. The clinically used anticancer drug doxorubicin served as the reference standard for comparison.

Antibacterial activity: The synthesised compounds **7a-l**, bearing different substituents at the R-position, were systematically evaluated for their antibacterial activity against selected Gram-positive bacteria, *Staphylococcus aureus* and *Bacillus subtilis* and Gram-negative bacteria, *Escherichia coli* and *Klebsiella pneumoniae*. The antibacterial screening was carried out at concentrations of 10 μg/mL and 20 μg/mL using the agar disc diffusion method, with gatifloxacin employed as the reference standard.

Antifungal activity: The synthesised compounds **7a-l**, containing different substituents at the R position, were evaluated for their *in vitro* antifungal activity against *Aspergillus niger*, *Aspergillus flavus* and *Fusarium oxysporum* at a concentration of 50 μg/mL using the agar disc diffusion method. The antifungal efficacy was expressed as the zone of inhibition (mm) and compared with the standard antifungal drug clotrimazole.

Molecular docking: Molecular docking is a computational technique widely used to predict the most favourable binding orientation of a ligand within the active site of a macromolecular target (receptor), leading to the formation of a stable complex. The epidermal growth factor receptor (EGFR) plays a crucial role in the progression of several types of cancer and is therefore considered a key therapeutic target in anticancer drug discovery. For this reason, the crystal structure of EGFR (PDB ID: 2J6M) was selected for *in silico* screening of the synthesised compounds.

Molecular docking studies were carried out using AutoDock Vina implemented through the PyRx virtual screening platform. The X-ray crystal structure of the epidermal growth factor receptor (EGFR) (PDB ID: 2J6M) [42] was obtained from the Protein Data Bank (www.rcsb.org). Ligand structures were constructed in ChemDraw Professional 16.0 and exported in MDL format. Prior to docking, the protein structure was prepared by removing co-crystallised water molecules and other non-essential heteroatoms, followed by the addition of polar hydrogen atoms. The processed protein was saved in PDBQT format. Ligands were subjected to geometry optimisation through energy minimisation and subsequently converted into .pdbqt format. Docking calculations were performed by defining a three-dimensional grid box encompassing the active site, with the exhaustiveness parameter set to 8 to ensure adequate conformational sampling. The docking poses and protein–ligand interactions were examined and illustrated using PyMOL and BIOVIA Discovery Studio.

RESULTS AND DISCUSSION

The target novel hydrazone-linked 1,2,3-triazole-pyrazole derivatives (**7a-l**) were successfully synthesized through a rational multistep sequence involving diazotisation, cycloaddition, hydrazone formation, Vilsmeier-Haack formylation and final condensation reactions. This synthetic route enabled efficient incorporation of three pharmacologically relevant heterocyclic motifs, namely triazole, pyrazole and sulfonyl hydrazone, within a single molecular framework. Initially, substituted aromatic anilines were transformed into the corresponding aryl azides (**2a-l**), which subsequently underwent base-mediated cycloaddition with a 1,3-dicarbonyl precursor to furnish substituted 1,2,3-triazole intermediates. The formation of pyrazole derivatives was then achieved through condensation of ketones (**3a-l**) with phenylhydrazine in ethanol using catalytic acetic acid, affording hydrazones (**4a-l**). Subsequent Vilsmeier-Haack formylation using DMF/$POCl_3$ introduced the aldehyde functionality at the desired position to yield carbaldehydes (**5a-l**). Finally, condensation of these aldehydes with benzenesulfonyl hydrazide in ethanol smoothly produced the target compounds (**7a-l**) in moderate to good yields (64-79%).

The structures of synthesised compounds **7a-l** were well supported by IR, NMR, mass spectrometry and elemental analysis. All derivatives exhibited characteristic absorption bands for the hydrazone N–H group in the 3202-3154 cm^{-1} region, confirming retention of the sulfonohydrazide proton. Aromatic =C–H stretching vibrations appeared near 3090-3021 cm^{-1}. Strong bands observed at 1715-1641 cm^{-1} were assigned to the azomethine (C=N) linkage formed during the final condensation step. Peaks in the range 1587-1526 cm^{-1} corresponded to aromatic C=C stretching vibrations. Bands at 1274-1225 cm^{-1} were attributed to the triazole-associated N=N/C–N vibrations, while strong absorptions around 1204-1112 cm^{-1} confirmed the presence of the sulfonyl (SO_2) group. These features collectively verified successful formation of the desired hydrazone-linked sulfonamide framework.

The proton NMR spectra of all compounds showed a characteristic singlet at δ 8.60-8.76 ppm assignable to the azomethine proton (–CH=N–), confirming hydrazone formation. Another singlet near δ 8.38-8.52 ppm corresponded to the NH proton of the sulfonohydrazide moiety. Multiplets and doublets between δ 7.06-7.91 ppm were due to aromatic protons of phenyl, substituted aryl and heteroaryl rings. Methyl-substituted derivatives displayed singlets near δ 2.30-2.75 ppm corresponding to aryl-CH_3 and triazole-CH_3 groups. Methoxy derivatives (**7e**, **7l**) showed distinct singlets around δ 3.89-3.94 ppm, confirming OCH_3 substitution. The carbon NMR spectra further supported the assigned structures. Signals for azomethine carbons appeared in the downfield region around δ 142-145 ppm. Methoxy-substituted compounds showed characteristic resonances near δ 55-56 ppm. Methyl carbons resonated around δ 10-22 ppm. Aromatic and heteroaromatic carbons were distributed across δ 114-140 ppm, consistent with substituted phenyl, pyrazole and triazole environments.

ESI-MS spectra displayed molecular ion peaks corresponding to $[M+H]^+$ for all derivatives, confirming their molecular masses. Representative examples included *m/z* 512 for **7a**, *m/z* 576 for brominated analogues (**7b**, **7j**), *m/z* 543 for nitro derivative **7c**, *m/z* 532 for chloro analogues (**7d**, **7h**), *m/z* 516 for fluoro derivatives (**7f**, **7k**) and *m/z* 528 for methoxy derivatives (**7e**, **7l**). These values were in excellent agreement with calculated molecular weights.

Cytotoxicity: Mostly derivatives showed lower toxicity toward the normal NIH/3T3 fibroblast cell line, indicating a degree of selectivity toward malignant cells. The IC_{50} values for both MCF-7 and NIH/3T3 cell lines are summarized in Table-1. All experiments were performed in triplicate and results were expressed as mean ± SD. Statistical significance was evaluated by one-way ANOVA at $p < 0.05$.

TABLE-1
IC_{50} VALUES (μM) FOR COMPOUNDS **7a-l**

Compound	IC_{50} ± SD (μM)			
	MCF-7	± SD	NIH/3T3	± SD
7a	2.11	0.23	12.09	0.88
7b	2.79	1.35	16.50	1.71
7c	0.55	0.86	8.55	1.08
7d	0.10	1.41	6.98	0.31
7e	4.41	0.16	13.84	1.74
7f	4.77	2.11	14.71	0.27
7g	0.69	1.22	5.50	0.51
7h	1.82	0.28	18.19	1.15
7i	3.06	1.50	19.84	1.45
7j	1.64	2.12	16.64	0.37
7k	5.21	2.57	16.40	1.10
7l	1.34	1.67	15.13	1.05
Doxorubicin	0.92	1.24	10.81	0.30

The cytotoxicity results indicated that both the electronic character and positional orientation of substituents at R-position significantly affected antiproliferative activity against the MCF-7 breast cancer cell line. In general, derivatives bearing electron-withdrawing groups demonstrated superior activity compared with analogues containing electron-donating substituents. Among the synthesised compounds, derivative **7d** carrying a *p*-chloro substituent showed the highest potency with an IC_{50} value of 0.10 μM, followed by compound **7c** containing a *p*-nitro group (IC_{50} = 0.55 μM). Both compounds exhibited stronger activity than the reference drug doxorubicin, which displayed an IC_{50} value of 0.92 μM under identical experimental conditions. These observations suggest that incorporation of electron-withdrawing groups at the *para*-position may enhance the cytotoxic potential of this scaffold. Nevertheless, considering the high potency observed, additional independent studies and rigorous statistical confirmation are required to verify reproducibility.

The unsubstituted derivative **7g** (R = H) also demonstrated significant activity (IC_{50} = 0.69 μM), indicating that substitution at the R-position is not essential for maintaining activity and that sterically neutral analogues remain effective. In contrast, compounds bearing electron-donating substituents such as *p*-methoxy and *p*-methyl generally showed reduced cytotoxicity suggesting that electron-rich aromatic substitution is less favourable for anticancer activity within this series.

Antibacterial activity: The antibacterial screening results revealed that the activity of compounds **7a-l** was significantly influenced by both the electronic nature and positional orientation of substituents at the R-position (Table-2). Derivatives bearing halogen substituents, particularly compounds **7b** (R = *p*-Br) and **7d** (R = *p*-Cl), exhibited significant antibacterial activity against Gram-positive strains such as *S. aureus* and *B. subtilis*, with inhibition zones comparable to the reference drug gatifloxacin (20 μg/mL) under identical experimental conditions. This trend suggests that electron-withdrawing halogens at the *para*-position favour enhanced interaction with Gram-positive bacterial targets.

Compounds containing electron-donating groups, including **7a** (R = *p*-Me) and **7e** (R = *p*-OMe), showed moderate to good antibacterial activity, although their potency was generally lower than that of the halogenated analogues. This indicates that electron-releasing substituents may support activity but are less effective in maximizing antibacterial response within this scaffold.

Among the *meta*-substituted derivatives, biological activity varied according to the substituent type. Compounds **7i** (R = *m*-Me) and **7j** (R = *m*-Br) displayed moderate antibacterial effects, whereas **7k** (R = *m*-F) showed comparatively improved activity against Gram-negative organisms, particularly *E. coli* and *K. pneumoniae*. In contrast, compound **7l** (R = *m*-OMe) exhibited relatively weaker activity. Compound **7c** (R = *p*-NO_2) also demonstrated selective inhibition against *E. coli* and *K. pneumoniae*, suggesting that the nitro group may enhance affinity toward certain Gram-negative strains.

The unsubstituted analogue **7g** (R = H) displayed moderate activity, indicating that substitution at the R-position is not essential for antibacterial action but contributes to improved the potency and selectivity. These results suggest that both electronic effects and substitution pattern play important roles in determining the antibacterial efficacy. Halogen substitution was particularly beneficial for Gram-positive activity, while selected *meta*-substituents improved Gram-negative inhibition. Among the synthesized series, compounds **7b**, **7d**, **7i** and **7k** emerged as the most promising antibacterial candidates for further biological investigation.

Antifungal activity: The observed activity indicated that both the electronic nature and positional orientation of the substituent at the R-position significantly influenced antifungal potency within this series. Compounds bearing electron withdrawing groups, particularly **7c** (R = *p*-NO_2) and **7f** (R = *p*-F), exhibited strong antifungal activity against the tested fungal strains, with inhibition zones comparable to the reference drug clotrimazole (Table-3). These findings suggest that *p*-positioned electron-withdrawing substituents favour enhanced interaction with fungal targets.

TABLE-2
ANTIBACTERIAL ACTIVITY OF COMPOUNDS **7a-l** AT DIFFERENT CONCENTRATIONS

Compound	Zone of inhibition (mm)							
	Gram positive bacteria				Gram negative bacteria			
	Stapylococus aeureus		*Bacillus Subtilis*		*Escherichia coli*		*Klebsiella pneumonia*	
	10 μg/mL	20 μg/mL	10 μg/mL	20 μg/mL	10 μg/mL	20 μg/mL	10 μg/mL	20 μg/mL
7a	16.2	21.5	17.1	12.5	14.1	17.5	19.1	14.5
7b	23.9	22.1	23.2	24.3	12.4	12.9	13.8	14.0
7c	13.6	12.6	14.6	13.4	22.4	19.2	19.4	21.5
7d	23.5	25.7	22.0	22.5	11.1	15.5	13.0	12.4
7e	13.5	14.2	15.2	16.2	13.8	14.5	12.6	13.8
7f	12.4	12.5	12.5	14.5	21.4	23.1	23.7	20.9
7g	13.5	14.5	14.5	14.8	18.6	18.4	15.8	16.1
7h	18.5	19.2	21.0	20.4	11.6	18.9	18.6	19.5
7i	20.3	21.7	21.0	21.2	13.5	12.1	11.0	14.1
7j	17.5	17.8	21.5	22.5	14.3	19.8	14.5	17.5
7k	10.2	10.4	16.0	10.4	21.4	27.4	26.5	23.9
7l	20.1	22.4	22.2	20.4	10.1	11.4	10.4	11.5
Gatifloxacin	20.2	22.7	19.8	22.1	16.2	17.5	17.9	10.5

TABLE-3
ANTIFUNGAL ACTIVITIES OF THE COMPOUNDS **7a-l** AT CONCENTRATION 50 μg/mL

Compound	Zone of inhibition (mm)		
	Aspergillus niger	*Aspergillus flavus*	*Fusariumoxy sporum*
7a	14.6	15.2	15.8
7b	19.8	17.9	18.7
7c	25.4	24.8	25.0
7d	14.9	19.8	19.8
7e	24.6	23.8	25.6
7f	25.9	26.2	24.8
7g	15.2	14.8	16.2
7h	23.4	22.5	24.5
7i	13.3	15.5	14.6
7j	17.6	16.8	18.6
7k	16.5	14.9	13.9
7l	19.8	20.8	20.8
Clotrimazole	17.3	20.4	21.2

The methoxy-substituted derivative **7e** (R = *p*-OMe) also demonstrated remarkable activity, indicating that antifungal potency in this scaffold is not governed solely by electronic withdrawal, but may also benefit from favourable steric or lipophilic effects. Among the *meta*-substituted analogues, compounds **7h** (R = *m*-Cl) and **7l** (R = *m*-OMe) showed moderate to good inhibition, whereas **7i** (R = *m*-Me) and **7k** (R = *m*-F) displayed comparatively lower activity. The unsubstituted analogue **7g** (R = H) showed only moderate antifungal effects, suggesting that aromatic substitution at the R-position contributes positively to biological performance. Based on the SAR, it is found that nitro, fluoro and methoxy substituents are valuable for antifungal activity in this molecular framework. Among the synthesized derivatives, **7c**, **7e** and **7f** emerged as the most promising candidates for further detailed biological investigation.

Molecular docking: The docking study revealed promising binding affinity values ranging from -8.5 to -10.2 kcal/mol, as shown in Table-4. To validate the docking protocol, the co-crystallised ligand AEE788 was re-docked into the active site of EGFR, yielding a binding energy of -9.8 kcal/mol with a RMSD value of 1.04 Å, confirming the reliability of the docking methodology. Among the screened compounds, ligands **7c** and **7d** exhibited the highest binding affinities toward EGFR, with docking scores of -10.2 and -10.1 kcal/mol, respectively. Both compounds demonstrated comparable binding modes, involving hydrogen bonding, van der Waals interactions, π-alkyl, π-cation and π-π stacking interactions. Fig. 1a illustrates the interaction of ligand 7c within the EGFR binding cavity, its interactions with key amino acid residues (Fig. 1b), and the three-dimensional binding conformation of the ligand (Fig. 1c). Notably, ligand **7c** formed significant interactions with critical EGFR residues, including Lys745, Asn842, Ile759, Lys875, Pro877, Val726, Leu718, Phe723 and Glu762.

TABLE-4
BINDING ENERGY VALUES FOR ALL THE SYNTHESISED COMPOUNDS **7a-l**

Ligand	Binding affinity	Ligand	Binding affinity
7a	-8.9	**7h**	-9.3
7b	-8.5	**7i**	-9.1
7c	-10.2	**7j**	-9.2
7d	-10.1	**7k**	-9.2
7e	-9.7	**7l**	-9.4
7f	-9.8	AEE788	-9.8
7g	-10.0		

Similarly, ligand **7d** exhibited strong interactions within the EGFR active site, as illustrated by its binding within the EGFR cavity (Fig. 2a), amino acid interactions (Fig. 2b), and three-dimensional binding orientation (Fig. 2c). Ligand **7d** formed hydrogen bonds and π-alkyl, π-cation and π-π stacked interactions with key residues such as Asp855, Asn842 (2.36 Å), Leu718 and Lys745. Among these, a notable π-π stacking interaction and a π-anion interaction involving Lys745 were observed, contributing to the enhanced binding stability. The reference ligand AEE788 exhibited hydrogen bonding interactions with Met793 and hydrophobic interactions with Ala743, Lys745, Leu844 and Thr790 within the EGFR binding pocket, as shown in Fig. 3. The docking poses of ligands **7c**, **7d** and AEE788 against EGFR (Figs. 1a and 2a) revealed significant overlap, indicating a similar binding orientation within the active site and suggesting comparable interaction patterns.

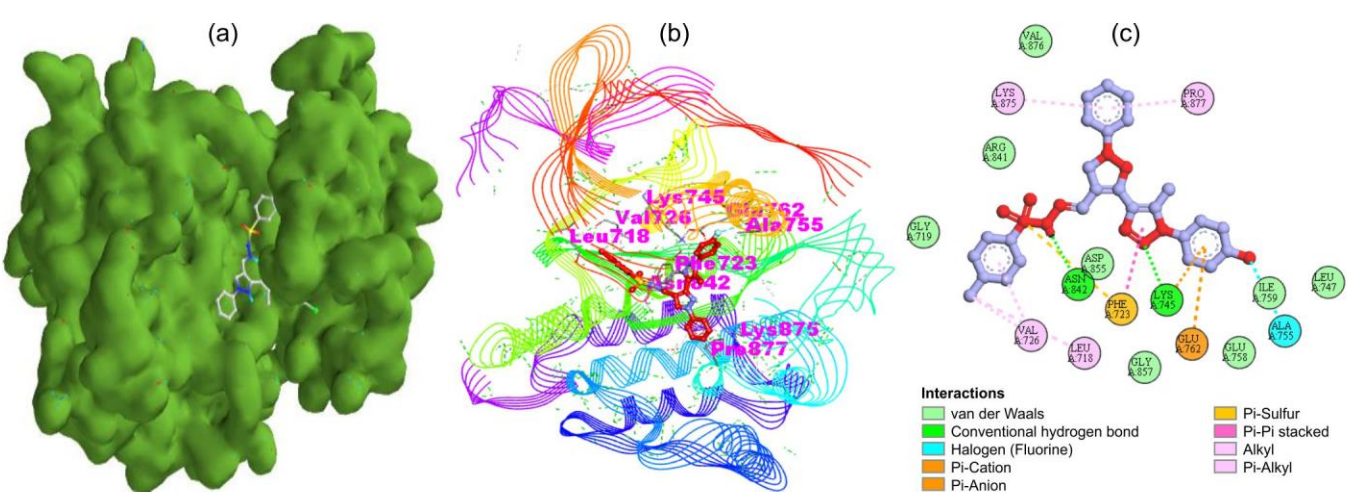

Fig. 1. Binding interactions of ligand **7c** against EGFR

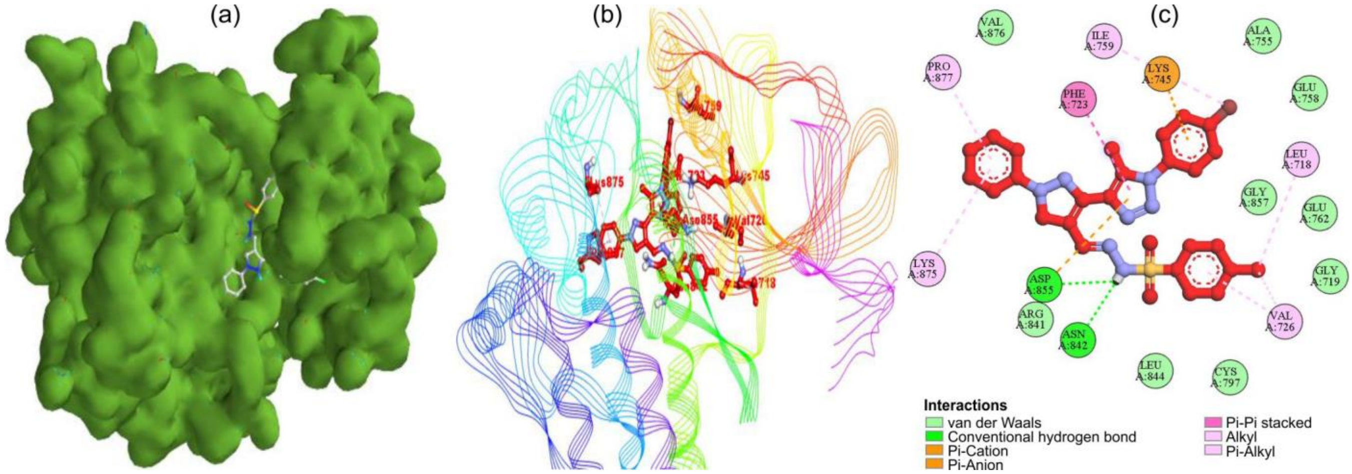

Fig. 2. Binding interactions of ligand **7d** against EGFR

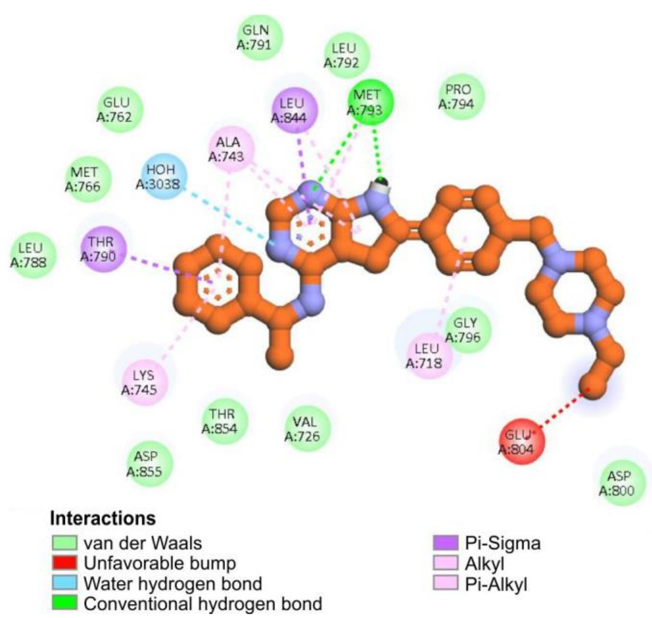

Fig. 3. Binding interactions of AEE788 against EGFR

The favourable docking scores and strong binding interactions observed for ligands **7c** and **7d** support their potential effectiveness as EGFR inhibitors. These *in silico* findings are in good agreement with the experimental results, highlighting the therapeutic relevance of the synthesised compounds.

Conclusion

A series of novel hydrazone-linked 1,2,3-triazole-pyrazole hybrids (**7a-l**) were synthesised and evaluated for their anticancer and antimicrobial activities. Several derivatives demonstrated remarkable *in vitro* antiproliferative activity against the MCF-7 cell line, with compounds **7d** (*p*-Cl) and **7c** (*p*-NO_2) showing the lowest IC_{50} values within the series under the tested conditions. The antibacterial evaluation indicated that halogenated and fluoro-substituted derivatives exhibited comparatively improved activity, while antifungal screening revealed favourable activity for nitro-, fluoro- and methoxy-substituted analogues. Preliminary SAR observations suggest that both electronic properties and positional substitution influence biological performance. Molecular docking studies indicated potential binding interactions with selected biological targets; however, further biochemical and mechanistic investigations are required to validate these findings.

ACKNOWLEDGEMENTS

The authors are thankful to the Head, Department of Chemistry, Osmania University, for providing research laboratory facilities, to CFRD, Osmania University, for analytical support and to University Grants Commission for financial assistance.

CONFLICT OF INTEREST

The authors declare that there is no conflict of interests regarding the publication of this article.

DECLARATION OF AI-ASSISTED TECHNOLOGIES

During the preparation of this manuscript, the authors used an AI-assisted tool(s) to improve the language. The authors reviewed and edited the content and take full responsibility for the published work.

REFERENCES

1. D. Lengerli, K. Ibis, Y. Nural and E. Banoglu, *Expert Opin. Drug Disc.*, **17**, 1209 (2022); https://doi.org/10.1080/17460441.2022.2129613
2. M.J. Vaishnani, S. Bijani, M. Rahamathulla, L. Baldaniya, V. Jain, K.Y. Thajudeen and I. Pasha, *Green Chem. Lett. Rev.*, **17**, 2307989 (2024); https://doi.org/10.1080/17518253.2024.2307989
3. D. Veeranna, L. Ramdas, G. Ravi, S. Bujji, V. Thumma and J. Ramchander, *ChemistrySelect*, **7**, e202201758 (2022); https://doi.org/10.1002/slct.202201758
4. R. Bhukya, M.K. Vanga, V. Thumma, A. Mudiraj, N. Ranjan, P.B. Phanithi and R. Jadhav, *J. Mol. Struct.*, **1349**, 143865, (2026); https://doi.org/10.1016/j.molstruc.2025.143865
5. A. Tan, *J. Mol. Struct.*. **1211**, 128060 (2020); https://doi.org/10.1016/j.molstruc.2020.128060
6. R. Gondru, S. Kanugala, S. Raj, C.G. Kumar, M. Pasupuleti, J. Banothu and R. Bavantula, *Bioorg. Med. Chem. Lett.*, **33**, 127746 (2021); https://doi.org/10.1016/j.bmcl.2020.127746

7. T.B. de Souza, I.S. Caldas, F.S. Paula, C.C. Rodrigues, D.T. Carvalho, and D.F. Dias, *Chem. Biol. Drug Des*., **95**, 124 (2020); https://doi.org/10.1111/cbdd.13628
8. R. Bhukya, M.K. Vanga, C. Bhukya, V. Thumma and R. Jadhav, *Chem. Biodiver.*, **22**, 3184, (2025); https://doi.org/10.1002/cbdv.202403184
9. M.C. Ríos and J. Portilla, *Chemistry*, **4**, 940 (2022); https://doi.org/10.3390/chemistry4030065
10. S. Mor, M. Khatri, R. Punia, S. Nagoria and S. Sindhu, *Mini-Rev. Org. Chem*., **19**, 717 (2022); https://doi.org/10.2174/1570193X19666220118111614.
11. E. Ameziane, I. Hassani, K. Rouzi, H. Assila, K. Karrouchi and M.H. Ansar, *Reactions*, **4**, 478 (2023); https://doi.org/10.3390/reactions4030029
12. A.A. Abu-Hashem, *J. Heterocycl. Chem*., **58**, 805 (2021); https://doi.org/10.1002/jhet.4216.
13. R. Matta, J. Pochampally, B.N. Dhoddi, S. Bhookya, S. Bitla and A. Gayatri, *BMC Chem.*, **17**, 61 (2023); https://doi.org/10.1186/s13065-023-00965-8.
14. M. Assali, M. Abualhasan, H. Sawaftah, M. Hawash and A. Mousa, *J. Chem.*, **2020**, 6393428 (2020); https://doi.org/10.1155/2020/6393428.
15. S.M. Jagadale, Y.K. Abhale, H.R. Pawar, A. Shinde, V.D. Bobade, A.P. Chavan, D. Sarkar and P.C. Mhaske, *Polycycl. Arom. Comp.*, **42**, 3216 (2020); https://doi.org/10.1080/10406638.2020.1857272
16. G.B.N.V.N. Kolukula, S. Subramanyam, T.R. Allaka and M.Z. Ahmed, *Chem. Biodiver.*, **22**, e202401810 (2025); https://doi.org/10.1002/cbdv.202401810
17. K.B. Gangurde, R.A. More, V.A. Adole and D.S. Ghotekar, *J. Mol. Struct*., **1299**, 136760 (2024); https://doi.org/10.1016/j.molstruc.2023.136760.
18. C.B. de Oliveira, J. França, T.C. LaPlante and S.R. Villar, *Mini-Rev. Org. Chem*., **20**, 342 (2020); https://doi.org/10.2174/1389557519666191014142448
19. E.R. Belyaeva, Y.V. Myasoedova, N.M. Ishmuratova and G.Y. Ishmuratov, *Russ. J. Bioorg. Chem*., **48**, 1123 (2022); https://doi.org/10.1134/S1068162022060085
20. D. Tzankova, S. Vladimirova, D. Aluani, Y. Yordanov, L. Peikova and M. Georgieva, *Acta Pharm.*, **70**, 303 (2020); https://doi.org/10.2478/acph-2020-0026
21. K.D. Katariya, S.R. Shah and D. Reddy, *Bioorg. Chem*., **94**, 103406 (2020); https://doi.org/10.1016/j.bioorg.2019.103406
22. S. Senthilkumar, J. Seralathan and G. Muthukumaran, *J. Mol. Struct*., **1226**, 129354 (2021); https://doi.org/10.1016/j.molstruc.2020.129354.
23. N. Fatima, A. Saeed, S. Ullah, S.A. Halim, A. Khan, M. Yaseen, M.Z. Hashmi, A. Mumtaz, H.R. El-Seedi, J. Uddin and A. Al-Harrasi, *Bioorg. Chem.*, **153**, 107822 (2024); https://doi.org/10.1016/j.bioorg.2024.107822
24. M. Marzi, M. Farjam, Z. Kazeminejad, A. Shiroudi, A. Kouhpayeh and E. Zarenezhad, *J. Chem*., **2022**, 7884316 (2022); https://doi.org/10.1155/2022/7884316
25. B. Sharma, S. Kumar, J. Preeti, M.D. Johansen, L. Kremer and V. Kumar, *Chem. Biol. Drug Des*., **99**, 301 (2022); https://doi.org/10.1111/cbdd.13984
26. S. Rollas and Ş.G. Küçükgüzel, *Molecules*, **12**, 1910 (2007); https://doi.org/10.3390/12081910
27. G. Verma, A. Marella, M. Shaquiquzzaman, M. Akhtar, M. R. Ali and M.M. Alam, *J. Pharm. Bioallied Sci*., **6**, 69 (2014); https://doi.org/10.4103/0975-7406.129170
28. B. Koçyiğit-Kaymakçıoğlu, E. Oruç, S. Unsalan, F. Kandemirli, N. Shvets, S. Rollas and A. Dimoglo, *Bioorg. Med. Chem. Lett*., **41**, 1253 (2006); https://doi.org/10.1016/j.ejmech.2006.06.009
29. B. Koçyiğit-Kaymakçıoğlu, E. Oruç, S. Unsalan, F. Kandemirli, N. Shvets, S. Rollas and A. Dimoglo, *Eur. J. Med. Chem.*, **38**, 1005 (2003); https://doi.org/10.1016/j.ejmech.2003.08.004
30. S.G. Agalave, S.R. Maujan and V.S. Pore, *Chem. Asian J*., **6**, 2696 (2011); https://doi.org/10.1002/asia.201100432
31. C.-H. Zhou and Y. Wang, *Curr. Med. Chem.*, **19**, 239 (2012); https://doi.org/10.2174/092986712803414213
32. H.C. Kolb, M.G. Finn and K.B. Sharpless, *Angew. Chem. Int. Ed.*, **40**, 2004 (2001); https://doi.org/10.1002/1521-3773(20010601)40:11<2004::AID-ANIE2004>3.0.CO;2-5
33. J.E. Moses and A.D. Moorhouse, *Chem. Soc. Rev*., **36**, 1249 (2007); https://doi.org/10.1039/B613014N
34. B. S. Holla, B. Veerendra, M. K. Shivananda and B. Poojary, *Eur. J. Med. Chem*., **37**, 511 (2002); https://doi.org/10.1016/S0223-5234(02)01358-2
35. S. Fustero, M. Sánchez-Roselló, P. Barrio and A. Simon-Fuentes, *Chem. Rev.*, **111**, 6984 (2011); https://doi.org/10.1021/cr2000459
36. A. Ansari, A. Ali and M. Asif, *New J. Chem*., **41**, 16 (2017); https://doi.org/10.1039/C6NJ03181A
37. J. Elguero, C. Marzin, A. R. Katritzky and P. Linda, The Tautomerism of Heterocycles, Academic Press, New York, p. 283 (1976).
38. A.A. Bekhit and T. Abdel-Aziem, *Bioorg. Med. Chem.*, **12**, 1935 (2004); https://doi.org/10.1016/j.bmc.2004.01.037
39. S. Kumar, S. Bawa and H. Gupta, *Mini Rev. Med. Chem.*, **9**, 1648 (2009); https://doi.org/10.2174/138955709791012247
40. K. Nepali, S. Sharma, M. Sharma, P.M.S. Bedi and K.L. Dhar, *Eur. J. Med. Chem*., **77**, 422 (2014); https://doi.org/10.1016/j.ejmech.2014.03.018
41. R. Morphy and Z. Rankovic, *J. Med. Chem.*, **48**, 6523 (2005); https://doi.org/10.1021/jm058225d
42. C.-H. Yun, T. J. Boggon, Y. Li, M. S. Woo, H. Greulich, M. Meyerson and M.J. Eck, *Cancer Cell*, **11**, 217 (2007); https://doi.org/10.1016/j.ccr.2006.12.017